# Spatial and temporal evolution of groundwater arsenic contamination in the Red River delta, Vietnam: Interplay of mobilisation and retardation processes

Emiliano Stopelli [a,*], Vu T. Duyen [b], Tran T. Mai [b], Pham T.K. Trang [b], Pham H. Viet [b], Alexandra Lightfoot [a], Rolf Kipfer [a], Magnus Schneider [c], Elisabeth Eiche [c], Agnes Kontny [c], Thomas Neumann [d], Martyna Glodowska [e,f], Monique Patzner [e], Andreas Kappler [e], Sara Kleindienst [f], Bhasker Rathi [g], Olaf Cirpka [g], Benjamin Bostick [h], Henning Prommer [i,j], Lenny H.E. Winkel [a,k], Michael Berg [a,l,*]

[a] Eawag, Swiss Federal Institute of Aquatic Science and Technology, Department Water Resources and Drinking Water, 8600 Dübendorf, Switzerland
[b] Key Laboratory of Analytical Technology for Environmental Quality and Food Safety Control (KLATEFOS), VNU University of Science, Vietnam National University, Hanoi, Vietnam
[c] Institute of Applied Geosciences, Karlsruhe Institute of Technology, 76131 Karlsruhe, Germany
[d] Applied Geochemistry, Institute for Applied Geosciences, Technical University Berlin, 10587 Berlin, Germany
[e] Geomicrobiology, Center for Applied Geosciences, University of Tübingen, 72076 Tübingen, Germany
[f] Microbial Ecology, Center for Applied Geosciences, University of Tübingen, 72074 Tübingen, Germany
[g] Hydrogeology, Center for Applied Geosciences, University of Tübingen, 72074 Tübingen, Germany
[h] Lamont-Doherty Earth Observatory, Columbia University, Palisades, 10964, NY, USA
[i] CSIRO Land and Water, 6014 Floreat, Western Australia, Australia
[j] School of Earth Sciences, University of Western Australia, Crawley, WA 6009, Australia
[k] Institute of Biogeochemistry and Pollutant Dynamics, ETH Zurich, 8092 Zurich, Switzerland
[l] UNESCO Chair on Groundwater Arsenic Within the 2030 Agenda for Sustainable Development, School of Civil Engineering and Surveying, University of Southern Queensland, QLD 4350, Australia

## HIGHLIGHTS

- Spatial and temporal arsenic evolution along 5 hydro(geo)chemical zones.
- Stable isotopes suggest groundwater recharge from river and evaporative sources.
- Significant arsenic (As) mobilisation in riverbank sediments.
- Highest dissolved As concentrations were found under methanogenic conditions.
- Pleistocene aquifer: sorption prevented As spread but redox changes are ongoing.

## GRAPHICAL ABSTRACT
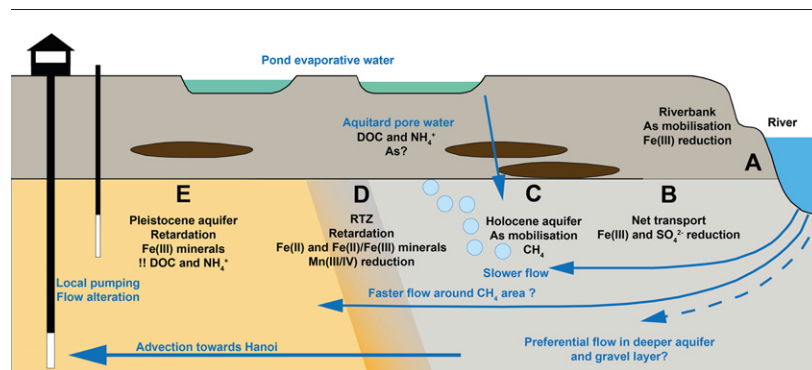


## ARTICLE INFO

## ABSTRACT

Geogenic arsenic (As) contamination of groundwater poses a major threat to global health, particularly in Asia. To mitigate this exposure, groundwater is increasingly extracted from low-As Pleistocene aquifers. This, however, disturbs groundwater flow and potentially draws high-As groundwater into low-As aquifers.

Here we report a detailed characterisation of the Van Phuc aquifer in the Red River Delta region, Vietnam, where high-As groundwater from a Holocene aquifer is being drawn into a low-As Pleistocene aquifer. This study

* Corresponding authors at: Swiss Federal Institute of Aquatic Science and Technology, Department Water Resources and Drinking Water, 8600 Dübendorf, Switzerland.
E-mail addresses: emiliano.stopelli@eawag.ch (E. Stopelli), michael.berg@eawag.ch (M. Berg).

includes data from eight years (2010–2017) of groundwater observations to develop an understanding of the spatial and temporal evolution of the redox status and groundwater hydrochemistry.
Arsenic concentrations were highly variable (0.5–510 μg/L) over spatial scales of <200 m. Five hydro(geo) chemical zones (indicated as A to E) were identified in the aquifer, each associated with specific As mobilisation and retardation processes. At the riverbank (zone A), As is mobilised from freshly deposited sediments where Fe(III)-reducing conditions occur. Arsenic is then transported across the Holocene aquifer (zone B), where the vertical intrusion of evaporative water, likely enriched in dissolved organic matter, promotes methanogenic conditions and further release of As (zone C). In the redox transition zone at the boundary of the two aquifers (zone D), groundwater arsenic concentrations decrease by sorption and incorporations onto Fe(II) carbonates and Fe(II)/Fe(III) (oxyhydr)oxides under reducing conditions. The sorption/incorporation of As onto Fe(III) minerals at the redox transition and in the Mn(IV)-reducing Pleistocene aquifer (zone E) has consistently kept As concentrations below 10 μg/L for the studied period of 2010–2017, and the location of the redox transition zone does not appear to have propagated significantly. Yet, the largest temporal hydrochemical changes were found in the Pleistocene aquifer caused by groundwater advection from the Holocene aquifer. This is critical and calls for detailed investigations.

## 1. Introduction

Geogenic arsenic (As) contamination of water resources is a global health issue that severely affects many regions in East, South and Southeast Asia (Berg et al., 2001; Winkel et al., 2008; Fendorf et al., 2010; Rodriguez-Lado et al., 2013; Podgorski et al., 2017). These are often densely populated regions, and groundwater is the main source of drinking water. Therefore, residents of these areas have a high risk of dietary exposure to As (Berg et al., 2007; van Geen, 2011). Continuous human exposure to As through water and food consumption can lead to serious chronic health problems ranging from cardiovascular diseases to cancer (Kapaj et al., 2006).

Geogenic As in groundwater results from the dissimilatory reductive dissolution of iron Fe(III) (oxyhydr)oxides in river and aquifer sediments by microbes, coupled to the oxidation of organic matter in anaerobic environments. These Fe(III)-reducing conditions are prevalent in Holocene river floodplains and in young river delta regions in East and South Asia. These zones often contain high levels of dissolved As and reduced, greyish sediments. A second type of aquifer is composed of older Pleistocene sediments, characterised by suboxic to moderately reducing conditions (usually manganese Mn(IV)-reducing), which preserve Fe(III)-bearing orange and brown sediments and have dissolved As concentrations below the WHO guideline value of 10 μg As/L (Harvey et al., 2002; McArthur et al., 2010; Hug et al., 2011; Postma et al., 2012; Lawson et al., 2013; van Geen et al., 2013). The sedimentary architecture between these two sediment types in river deltas is often complex, with Holocene aquifers both vertically overlying and laterally adjoining aquifers of Pleistocene age. The transition zones between the Holocene and Pleistocene aquifers are generally marked by a change from highly to moderately reducing conditions, constituting a redox transition zone (RTZ). When As-enriched water from the Holocene aquifer migrates into the Pleistocene aquifer, the As migration is retarded by enhanced sorption onto (i) Fe(III) (oxyhydr)oxides, which are characterised by high surface areas and which are significantly more abundant in Pleistocene sands (Rathi et al., 2017; Neidhardt et al., 2018ba; Sø et al., 2018a); and (ii) authigenic minerals produced by redox reactions in the RTZ (e.g., Rawson et al., 2016; Rawson et al., 2017) or by other as yet undefined incorporation processes. However, the RTZ is expected to move as a consequence of the induced advection of Holocene groundwater caused by the massive groundwater abstraction from currently uncontaminated deeper Pleistocene aquifers (McArthur et al., 2010; van Geen et al., 2013). The rate at which RTZs migrate and the actual processes that govern the migration rates are still poorly understood (Polya and Charlet, 2009). A further puzzling question concerns the causes of the observed spatial patchiness of As contamination in the wells used for drinking water extraction. Despite progress in the broad-scale ($10^4$–$10^6$ m) prediction of risk areas of

geogenic As contamination (Winkel et al., 2008; Winkel et al., 2011; Podgorski et al., 2017), the relative impact of natural and anthropogenic factors on the local-scale ($10^1$–$10^3$ m) variability of dissolved As concentration, as well as the variability in neighbouring wells, remains largely unknown (Berg et al., 2008; Richards et al., 2017; Polya et al., 2019).

Here, we report and analyse a time series of water hydrochemistry and stable isotopic composition data collected between 2010 and 2017 in the Red River Delta Region, Vietnam. The study site features conditions representative of East and South Asian regions, with adjoining Holocene and Pleistocene aquifers of distinctly different redox conditions (Berg et al., 2008; Eiche et al., 2008; van Geen et al., 2013). The site is also characterised by an advective groundwater flow from the high-As (Holocene) into the low-As (Pleistocene) aquifer. This is a consequence of extensive groundwater pumping from Pleistocene aquifers by the city of Hanoi and a resultant reversal of the natural groundwater flow direction. These steady flow conditions allow an integration and comparison of long-term hydrochemical data obtained from monitoring campaigns conducted since 2010. This comprehensive dataset allowed us to (i) constrain the sources of water feeding the aquifer; (ii) assess the hydro(geo)chemical characteristics of our site and determine mobilisation and retardation processes responsible for the spatial variability of dissolved As; (iii) study the temporal evolution of As and other relevant hydrochemical parameters along the redox gradient from the Holocene to the Pleistocene aquifer; (iv) assess whether the RTZ is migrating under advection; and (v) simplify and summarise the interplay of As (im)mobilisation processes into 5 major hydro(geo) chemical zones with unique geochemical features.

## 2. Materials and methods

### 2.1. Study site

The study site is located near Van Phuc village, Vietnam, on a meander of the Red River, about 15 km southeast of Hanoi (Fig. 1a and b). The site is characterised by features (Fig. 1c) that make it particularly suitable for studying As transport behaviour, and it is representative of many groundwater systems in the South and East Asian regions (Berg et al., 2008; Eiche et al., 2008; van Geen et al., 2013; Stahl et al., 2016). Above all, it features a Holocene aquifer that is characterised by reducing conditions and high dissolved As concentrations and that lies adjacent to a Pleistocene aquifer that is characterised by low concentrations of As and less reducing conditions. The stratigraphy is distinguished by a top layer of Holocene silty sediments (grain size <63 μm) with a minor content of clays (<2 μm), constituting an aquitard on top of the aquifer with a thickness of 15–22 m (from ground level to the aquifer). The aquitard is intercalated with peat layers enriched in organic matter derived from
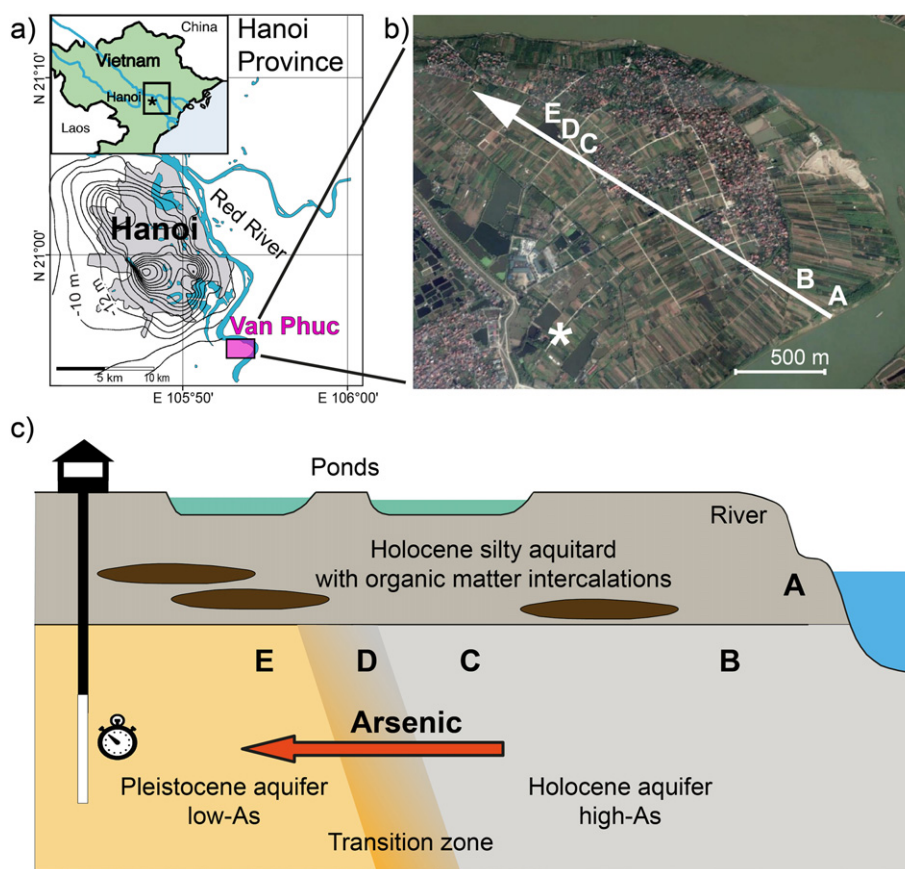
**Fig. 1.** a) Location of Van Phuc village situated at the Red River in the Hanoi region. Contour lines show the groundwater heads of the Pleistocene aquifer in 2008 that illustrate the extensive groundwater abstractions in Hanoi (Berg et al., 2008; van Geen et al., 2013). b) Satellite image (Dec. 2014, Google Earth) of the study site, with the dominant groundwater flow direction marked by the white arrow, along which most of our studied groundwater observation wells are located. The letters represent the major hydro(geo)chemical zones, as discussed in the paper: A = riverbank; B = Holocene well closest to the river; C = Holocene aquifer; D = redox transition zone (RTZ); E = Pleistocene aquifer. The star indicates the location of a well surrounded by ponds outside the studied transect. c) Schematic features of the study site, with the connection of grey Holocene and orange Pleistocene sands separated by the RTZ (gradient grey-orange).

the burial of marine and riverine plant remains and swamps (Tanabe et al., 2003; Eiche et al., 2017). The Holocene aquifer that lies underneath (from 15 to around 55 m depth) is mainly composed of reduced grey sands (>63 μm and <2 mm) and silts with mixed $Fe(II)/Fe(III)$ valence minerals, while the adjacent Pleistocene aquifer (from 18 to around 45 m depth) is composed of orange-brown Pleistocene sands and silts dominated by $Fe(III)$ (oxyhydr)oxides (Eiche et al., 2008; van Geen et al., 2013). A layer of oxidised clays-silts between the Pleistocene aquifer and the Holocene silty aquitard has been previously observed and identified as paleosol (van Geen et al., 2013).

The municipal waterworks of the region abstracts and supplies water from the deeper Pleistocene aquifers below Hanoi to avoid exposing the inhabitants of Hanoi to As-contaminated drinking water. However, a substantial population increase in the Hanoi region over the last century has caused a massive increase in groundwater extraction. For example, in 2017, the total daily groundwater extraction was approximately 1,000,000 m³/day (Giao et al., 2018). This extraction has resulted in large cones of depression in both the Holocene and Pleistocene aquifers beneath Hanoi and the surrounding areas (Fig. 1a). As a consequence, the groundwater flow direction in Van Phuc has changed from a natural northwest to southeast gradient to an induced direction from southeast to northwest towards Hanoi (Fig. 1b, Berg et al., 2008; Winkel et al., 2011), at an estimated average velocity of 40 m/year (van Geen et al., 2013). Based on groundwater dating, this reversal of the flow direction most likely occurred 50–60 years ago (van Geen et al., 2013) and has led to the intrusion of groundwater from the Holocene into the Pleistocene aquifer.

### 2.2. Sample collection and preservation

An electric submersion pump was used to collect groundwater from 19 wells in Van Phuc village in October 2017. Samples were taken after at least 10 min of pumping, when the daily-calibrated field multiprobe WTW 3630 indicated a stable oxygen concentration (FDO 925-3), conductivity (TetraCon 925-3) and redox potential (ORP 900-P). Values recorded by the ORP electrode were converted and are presented with reference to the standard hydrogen electrode SHE potential, indicated hereafter as $E_h$. The pH and temperature were also recorded (SenTix 940-3 sensor). Pumped water was collected into a pre-rinsed bucket to allow mixing, while avoiding turbulence. Alkalinity was determined as $HCO_3^-$ in the field (Merck alkalinity test kit Mcolortest 11109). Water samples from the Red River and ponds were taken directly using a bucket, and the field parameters ($O_2$, pH, $E_h$, conductivity and temperature) were measured immediately. Riverbank pore water was collected using a method adapted from Stahl et al. (2016). Briefly, samples were collected by using a custom-made stainless steel rod (outer diameter 1 cm, inner diameter 7 mm, 1 m in length; clogging was prevented by a 4 cm screen with 1 mm holes protected by a finer mesh around the top of the rod), which was inserted 25–30 cm deep into the riverbed, close to the contact between the river water and the riverbank. Water was extracted with a syringe, which was plugged into a plastic tube inserted into the inner part of the rod. The water was then subdivided into aliquots for analyses. Field parameters were not measured for riverbank samples because the volumes were too small.

All samples were collected in Nalgene polypropylene bottles, and several aliquots were taken for separate analyses. The aliquot (50 mL) for metals and trace elements, $PO_4^{3-}$ and ammonium $NH_4^+$, was filtered (0.45 μm cellulose acetate syringe disposable filters, BGB Analytik, both filters and bottles pre-rinsed with 10 mL sample) and acidified in the field to pH <2 with 1% v/v $HNO_3$ (Merck, Suprapur quality grade). An aliquot for As(III) determination (30 mL) was collected by passing the sample through a disposable As(III)/As(V) separation cartridge (MetalSoft, Meng and Wang, 1998) after the filtration step and before acidification. The aliquot for dissolved organic carbon (DOC, 50 mL) was also filtered but was acidified in the field to pH <2 with 1% v/v HCl (Merck, Suprapur quality grade). Anions ($NO_3^-$, $SO_4^{2-}$, $Cl^-$, $Br^-$), total dissolved nitrogen DN and alkali cations ($Na^+$, $K^+$, $Ca^{2+}$, $Mg^{2+}$) were determined in a filtered (0.45 μm cellulose acetate), non-acidified aliquot (120 mL). Finally, 8 mL samples were collected, without headspace, in amber glass vials for the determination of $\delta^2H$ and $\delta^{18}O$. Immediately after collection, all aliquots were stored at 4 °C protected from light until analyses. Samples for methane determination were collected directly from the pumping tube to minimise the risk of degassing by inserting a needle into evacuated glass vials (Labco 819W). A headspace of half to two-thirds of the total volume was left, and the vials were immediately frozen on dry ice in an upside down position to ensure trapping of the gas phase above the frozen water in the vial headspace.

## 2.3. Water analyses and quality assurance

All measured parameters are presented in Table A1. The major cations and trace elements were determined by inductively coupled plasma mass spectrometry (ICP-MS; an Agilent 7500 system equipped with a reaction cell). As, Br, P and S were further quantified with an ICP-MS/MS system (Agilent 8900). Reference materials NIST 1643f, a Fluka primary multi-anion standard solution and an internal reference solution ARS-29 were intermittently analysed to guarantee the robustness of the analyses. For the ICP-MS, the calibration curves were $r^2 > 0.999$, and standard deviations of the triplicate analyses were <5%. Concentrations of $NH_4^+$ and $PO_4^{3-}$ were determined by photometry via the indophenol and molybdate methods, respectively. DOC was analysed by catalytic combustion and an infrared (IR) $CO_2$ detector on a total C and N analyser (Shimadzu TOC-L CSH). DN was quantified using the same instrument, equipped with an ozonation module after sample combustion and a UV detector for $NO_x$. Anions and cations were determined by ion chromatography (Metrohm 761 Compact IC). Comparisons of total dissolved concentrations of N, P and S were generally equivalent to $NH_4^+$, $PO_4^{3-}$ and $SO_4^{2-}$. Given the neutral pH and reducing conditions, most of the dissolved Fe should be present as $Fe^{2+}$. This was confirmed with screening measurements carried out in April 2018, when $Fe^{2+}$ was measured photometrically with ferrozine directly in field and determined to constitute ≥92% of total dissolved Fe.

Stable water isotopes were analysed using a Picarro cavity ringdown spectrometer. The Limit of Quantification (LOQ) of each measurement is provided in Table A1 in the Appendix. Methane concentration was determined using GC-2014 (Shimadzu), equipped with a Porapak T packed column and a flame ionisation detector using the headspace equilibration method and the procedure of Sø et al., 2018b. Cross-contamination between the collection of two successive water samples was minimised by rinsing the syringes twice with deionised water and twice with the new sample. Field blanks were also collected routinely to check for possible contamination during sampling. These blanks were obtained by first rinsing the syringes twice (cleaning) and then twice again (as a new sample) using deionised water; deionised water was then collected for the aliquot sub-samples. The field blank values were below or equal to the LOQs for all the parameters measured except for DOC. The field blank values for DOC were, on average, 0.2 mg/L above the LOQ; therefore, the concentrations in the samples were corrected for this value. Several elements were analysed as duplicates, allowing

further assurance of analytical quality and comparability among the different methodologies. Na, Ca, Mg and K were analysed by ICP-MS (elements) and IC (ions), with concentrations measured by IC within 5% of elemental concentrations determined by ICP-MS and with an $R^2 > 0.96$. The same performance quality was obtained for the concentrations of As and P, analysed twice with ICP-MS 7500 and 8900, and for $NH_4^+$ and $PO_4^{3-}$, analysed independently by photometry in two laboratories.

## 2.4. Geochemical modelling and statistical analyses

Mineral saturation indices were calculated with PHREEQC (v3.4.0-12927, Parkhurst and Appelo, 2013) using the minteq.v4.dat database. Model calculations included all measured relevant major, trace and redox-sensitive solutes (Table A1). Field-measured values of temperature and pH were included, and the measured redox potentials $E_h$ were converted into electron activity ($pe_{Eh}$) using the Nernst equation (Appelo and Postma, 2005). The saturation indices (SI, Table A3) of the major mineral phases were initially calculated for groundwater samples collected in October 2017, assuming redox equilibrium values of the $Fe^{3+}/Fe^{2+}$, $SO_4^{2-}/H_2S$ and $Mn^{4+}/Mn^{2+}$ systems at the measured redox potential. A SI > 0 indicates oversaturation of groundwater with respect to a mineral, implying the mineral is stable and either forming or present in the solid phase; while a SI < 0 indicates undersaturation and either the absence or kinetic metastability of the mineral. Under the prevailing field conditions, Fe and S could precipitate from groundwater, resulting in lower concentrations in solution and ultimately in an underestimation of the effective SI. Furthermore, not all redox couples could be necessarily at full equilibrium. Therefore, a range of different model scenarios was assessed by imposing equilibrium with either FeS, pyrite, ferrihydrite, or goethite, and the concentrations of solutes subsequently re-calculated (Table A3). If no major change occurred in the calculated groundwater composition, this implied that the solution was in equilibrium with the mineral. Any increase in the modelled dissolved $Fe^{2+}$ and/or $SO_4^{2-}$ concentrations implied undersaturation of groundwater with respect to the mineral at the time the sample was taken and that the mineral was most likely not present or not very reactive. Dissolved inorganic carbon (DIC) concentrations have been calculated as well (Table A3), and are correlated with C-alkalinity ($R^2 = 0.97$, DIC = 1.19 · C-alkalinity).

Parametric, non-parametric and multi-parametric statistical tests and probability calculations were carried out using the PAST software, version 3.17 (Hammer et al., 2001).

## 3. Results and discussion

### 3.1. Aquifer water sources based on $^{18}O$ and $^2H$ isotopes in water

Stable water isotope signatures ($\delta^2H$ and $\delta^{18}O$) in the groundwater and surface water samples were analysed to determine the contribution of different water sources to the groundwater composition. Potential sources of groundwater are: Red River water (blue, Fig. 2), rain water (black, Fig. 2, data from Berg et al., 2008) and pond water infiltrate (green, Fig. 2).

The $\delta^2H$ and $\delta^{18}O$ values in Fig. 2 show that (i) pond water samples are highly impacted by evaporative processes and therefore deviate considerably from the local meteoric water line (LMWL, $\delta^2H = 9.9 \, \delta^{18}O + 27$, Berg et al., 2008), and (ii) the isotopic signatures of the ponds show a high seasonal variability ($\delta^{18}O$ from −8.1 in autumn to −2.7‰ in spring, $\delta^2H$ from −55 to −18‰). Artificial ponds are a common feature of this region and are generally used for aquaculture, including duck, fish and water plant farming. They are regularly refilled with water pumped from the Red River and are then exposed to successive periods of evaporation. By contrast, Red River water generally has a more stable isotope signature, not only during the course of a year ($\delta^{18}O$ from −9.6 to −8.8‰, $\delta^2H$ from −66 to −61‰ between 2017 and 2018), but also across
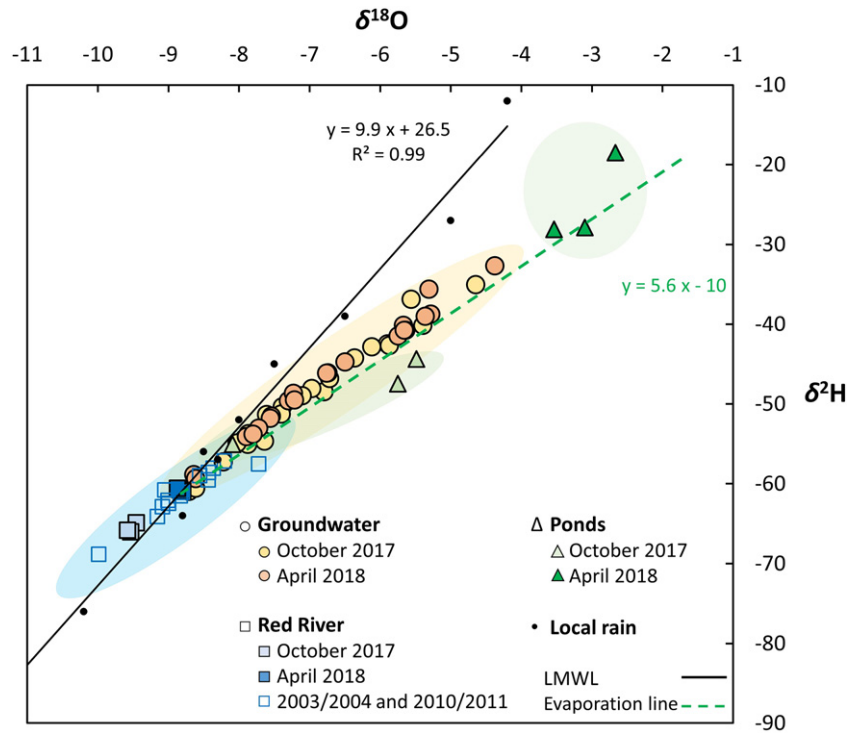
**Fig. 2.** $\delta^2$H versus $\delta^{18}$O‰ Vienna Standard Mean Ocean Water (VSMOW) values in: precipitation (local meteoric water line LMWL, black line, data from Berg et al., 2008); Red River water (blue squares); pond water (green triangles); local evaporation line (in green, data from Berg et al., 2008); groundwater and riverbank samples (orange circles).

different years, and this signature is predominantly impacted by rainfall (values along the LMWL). Isotopic values of groundwater samples (yellow and orange dots in Fig. 2) were more similar between the dry (November–April) and wet (May–October) monsoon seasons. The corresponding isotope data all plotted along the local evaporation line (from Berg et al., 2008), which coincides with the mixing line of the isotopic values of the river water with those of the pond water. This indicates that the groundwater consists of a mixture of evaporated surface water and river water, which is in line with regional trends (Nghiem et al., 2019).

The 2-D representation of the $\delta^{18}$O values (Fig. 3), complemented with previously determined groundwater age data (van Geen et al., 2013), provides useful constraints for defining the key hydrological patterns. The data suggest that river water infiltrates at the riverbank (A), through the Holocene aquifer (B and C) towards the redox transition zone (D), particularly at 30 to 45 m depth. Samples at a depth of 25 to 30 m within the Holocene aquifer, across the RTZ and in the Pleistocene sands (E) show higher evaporative $\delta^{18}$O values. Previous studies at the same site (Eiche et al., 2008) reported the presence of a gravel layer below the sandy aquifer at a variable depth of 45 to 55 m. Samples
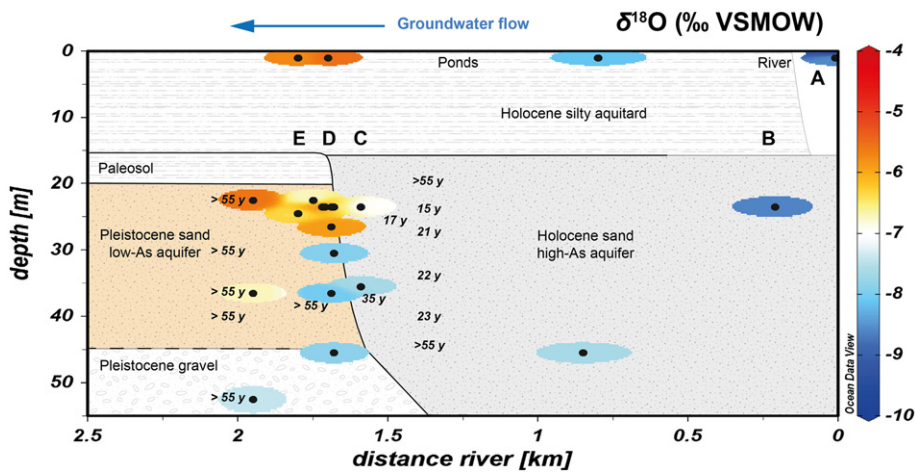


**Fig. 3.** Two dimensional cross-section of groundwater $\delta^{18}$O‰ VSMOW values in October 2017, Van Phuc village. Following the groundwater flow from right to left, the capital letters A-E mark the identified major hydro(geo)chemical zones, as indicated in Fig. 1. The black dots indicate the positions of the monitored groundwater wells, and the coloured shading is based on weighted-average gridding interpolation of well data realised using Ocean Data View (https://odv.awi.de). The different sediment types are indicated, and are marked by different colours for the aquifer. The dashed line represents the discontinuous presence of clay deposits between the Pleistocene aquifer and the gravel layer below. Apparent groundwater ages, based on $^3$H-$^3$He data from 2006, are reported in italics. (For interpretation of the references to colour in this figure, the reader is referred to the web version of this article.)
(data from van Geen et al., 2013).

from wells screened in the gravel layer show $\delta^{18}O$ values in the range of river water, probably indicating that river water reaches the coarser sediments below the sandy aquifers.

Given the presence of a clayey silt depositions overlying the sandy sections of the Holocene aquifer (Eiche et al., 2008), the evaporative signature found in aquifer samples is somewhat unexpected. One possible explanation is that surface evaporative water has been percolating through preferential flow paths into the underlying aquifer (Lawson et al., 2013; Kuroda et al., 2017a). This may have occurred (i) along intercalated sand lenses of variable thickness embedded in the aquitard; these lenses were previously reported (Eiche et al., 2008) and found to result from a succession of several riverine and estuarine sediment depositions (Tanabe et al., 2003; Eiche et al., 2017), and/or (ii) by leaking artificial pond bottoms (Harvey et al., 2002; Lawson et al., 2013). The prevalence of older groundwater at a depth of 20 m in the Holocene aquifer on top of younger water infiltrated from the Red River (Fig. 3) provides support for the slow percolation of water across discontinuities in the silty aquitard. In some cases, pond water does appear to reach the aquifer; for example, the well indicated with a star in Fig. 1b is located off the transect, in an area of ponds, and has evaporative isotopic values that best match those of the ponds, despite being only about 650 m away from the river ($\delta^{18}O = -4.4/-4.6‰$; $\delta^2H = -33/-35‰$). The silty aquitard could itself also contain water that is linked to both evaporative riverine and estuarine sedimentary phases, in the form of cut-off meanders and mangrove swamps.

## 3.2. Spatial distribution of arsenic contamination and hydro(geo)chemistry

### 3.2.1. Dissolved arsenic

In the samples collected in the post-monsoon season in October 2017, dissolved As concentrations ranged from 0.5–509 µg/L (Fig. 4 and Table A1). Overall, 53% (10 of 19) of the wells exceeded the guideline value of 10 µg/L for As, with the highest concentration exceeding the WHO limit by up to 50 times (WHO, 2011). Furthermore, 58% of the samples exceeded the health-based value of 2 mg/L for iron (Fe), and 74% exceeded the health-based value of 0.4 mg/L for manganese (Mn) (WHO, 2011). Concentrations of dissolved As decreased sharply at the RTZ between the Holocene and Pleistocene aquifers within a longitudinal distance between wells of <200 m. Throughout the Holocene aquifer, As was predominantly present as As(III) (90–96% of total As).

Considering the whole set of riverbank and groundwater samples (Table A2, n = 21), As correlates with Fe ($r_s = 0.72$), $PO_4^{3-}$ ($r_s =$ 0.70), methane $CH_4$ ($r_s = 0.70$), dissolved organic carbon DOC ($r_s =$ 0.65), conductivity ($r_s = 0.51$), C-alkalinity ($r_s = 0.50$) and ammonium $NH_4^+$ ($r_s = 0.46$). Furthermore, As correlates inversely with the redox potential $E_h$ ($r_s = -0.86$) and Mn ($r_s = -0.43$). These correlations suggest that the presence of organic matter is promoting the reduction of Fe(III) (oxyhydr)oxides, with the concomitant mobilisation of sorbed As and $PO_4^{3-}$. In addition, the distributions of As, Fe and $PO_4^{3-}$ in solution over the whole cross section (Figs. 4 and A2) indicate that precipitation of Fe in Pleistocene sediments is leading to a removal of As and $PO_4^{3-}$ from solution by sorption and/or incorporation (Rathi et al., 2017; Neidhardt et al., 2018ba; Neidhardt et al., 2018ab). Additionally, enough organic carbon must be present in the aquifer to concomitantly reduce Fe, mobilise As and stimulate methane production. Similarly, adsorption processes that remove As from solution must be accompanied by parallel processes, which consume methane for the As-methane correlations to persist across the redox transition. The negative correlation between As and Mn distribution over the cross section (Fig. A2) suggests that Mn(III/IV) (oxyhydr)oxides reduction is occurring in wells where Fe(III)-reduction is not yet occurring and where As concentrations are still low or decreasing. This results in the production of dissolved Mn concentrations up to 3.9 mg/L (Buschmann et al., 2008; McArthur et al., 2010). The increase in dissolved Mn concentrations in wells could be an effective early indicator of future increases in As.

Interestingly, upon combining the parameters that best correlated with As (Table A2), the linear combination of the redox potential $E_h$ and $PO_4^{3-}$ provided one of the best models and described >90% of all the variability of As concentrations observed in the wells of Van Phuc village. The empirical relation is given by:

$$\log As \; µg/L = 0.9 \cdot \log PO_4^{3-} \; mg/L - 0.009 \cdot E_h + 2.86$$

(adjusted multivariate $R^2 = 0.91$, $p_{tot} < 0.001$, $p_{x1} < 0.001$ $p_{x2} = 0.001$, Fig. A1). Despite the limited amount of site-specific observational data, this type of equation could be useful for monitoring dissolved As in aquifers where the behaviour of Fe minerals is a linear function of $E_h$. This could happen, for instance, where marked Fe(III) reduction and methanogenic conditions are present together with low sulphate concentrations (Sracek et al., 2018). Under these conditions, the redox potential $E_h$ and $PO_4^{3-}$ can work as proxies of the geogenic As release under reducing conditions and of the sorption properties of As, respectively. These parameters are also easily measured with sensors ($E_h$) and by photometry ($PO_4^{3-}$). Thus, a similar empirical relationship can provide
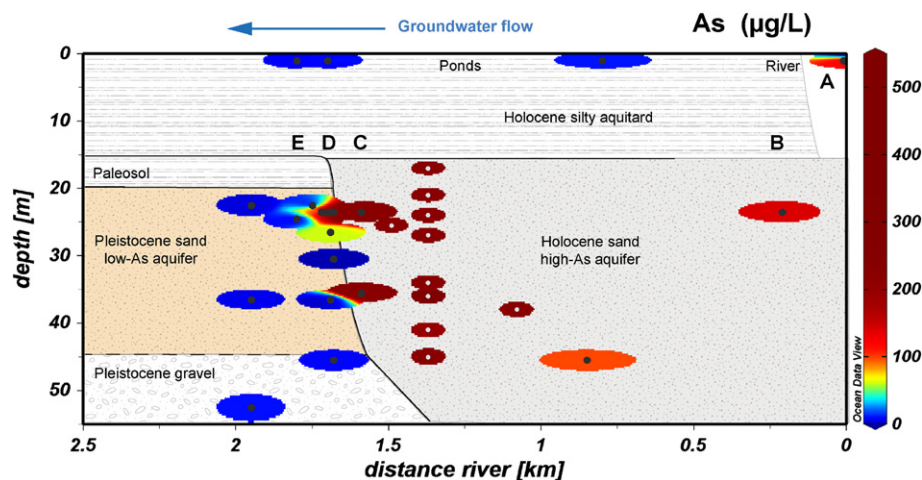


**Fig. 4.** Two-dimensional cross-section of dissolved As concentrations in October 2017, Van Phuc village. Further parameters are shown in Figs. A2 and A3. Following the groundwater flow from right to left, the capital letters A–E mark the identified major hydro(geo)chemical zones, as indicated in Fig. 1. The black dots indicate the positions of the monitored groundwater wells, and the coloured shading is based on weighted-average gridding interpolation of well data realised using Ocean Data View (https://odv.awi.de). The smaller ellipses with white dots represent dissolved As concentrations measured in the Holocene aquifer in 2006, as reported in Eiche et al. (2008). The different sediment types are indicated and are marked by different colours for the aquifer. The dashed line represents the discontinuous presence of clay lenses between the Pleistocene aquifer and the gravel layer below.

an early and simple screening assessment of the risk of As contamination in other sites where continuous As measurement is not possible.

### 3.2.2. Mineral saturation indices

Calculated saturation indices (SI) of riverbank and groundwater samples (Table A3) indicate dominant Fe(III)-reducing conditions at the site, similar to those reported by Sracek et al. (2018) for the Red River Delta in Vietnam and Richards et al. (2017) for a site in Cambodia. At the riverbank (A), simulation results show reducing conditions and undersaturation of groundwater with respect to Fe(III) (oxyhydr)oxides, such as ferrihydrite and goethite, thereby favouring the kinetically controlled formation of mixed-valent Fe(II)/Fe(III) (oxyhydr)oxides, such as magnetite ($SI_{ferrihydrite} = -5.2$, $SI_{goethite} = -2.5$, $SI_{hematite} = -2.6$, $SI_{magnetite} = 1.5$). Following the groundwater flow path from the Holocene into the Pleistocene aquifer (zones B to E), the modelled $SI_{ferrihydrite}$ is between $-1$ and $-2$, $SI_{goethite}$ is around $0-1$ and $SI_{hematite}$ is >1. These values are in agreement with the potential depletion of poorly crystalline Fe(III) minerals, such as ferrihydrite, and the presence of more crystalline Fe(III) (oxyhydr)oxides, like goethite and hematite. The calculated saturation indices also indicate the likelihood of the formation of Fe(II)/Fe(III) (oxyhydr)oxides and Fe(II) carbonates ($SI_{magnetite} > 5$, $SI_{siderite}$ around 0). The hydrochemical data and calculated saturation indices jointly suggest that sulphate reduction to sulphide occurs in zone A (riverbank), with sulphides subsequently precipitating as Fe-sulphide minerals along the flow path. Pyrite is still oversaturated ($SI_{pyrite} = 7-9$) in zone A, possibly due to kinetic limitations, whereas equilibrium conditions are reached further downstream in zone B ($SI_{pyrite} = 0.2$). In zones C to E, iron sulphide minerals are undersaturated, suggesting their depletion at those locations. In the Pleistocene aquifer (wells A-24, A-38, Tables A1 and A3), no or only

insignificant changes occur in the groundwater composition when imposing equilibrium with pyrite, indicating saturation conditions of groundwater with respect to this mineral. SI reported in this study are coherent with previous mineralogical characterisations carried out in Van Phuc (Eiche et al., 2008).

### 3.2.3. Hydro(geo)chemical zones critical for As mobilisation and retardation

We used the joint interpretation of the various data types to determine five specific hydro(geo)chemical zones (A–E) that are identified as the most critical aquifer sections in terms of controlling the observed arsenic concentration patterns. For our discussion, we focus our analysis on the wells screened between 22 and 25 m, which is the depth at which the highest dissolved As concentrations are found (Table 1).

Within the first few centimetres of shallow riverbank sediments (zone A), the freshly deposited organic matter (OM) is oxidised, as indicated by the Mn(IV)- and Fe(III)-reducing conditions in pore water at just 25–30 cm depth (dissolved concentrations of Fe and Mn 1.4–12 mg Fe/L and 5.7–8.8 mg Mn/L, respectively). This oxidation of OM is also confirmed by the high C-alkalinity and DIC values and the observed release of C, N and S into solution (Table 1). The reductive dissolution of Fe(III) (oxyhydr)oxides is associated with the presence of elevated As concentrations in the riverbank pore water (77–169 μg/L); 90% of this is present as As(III), consistent with values published previously (Stahl et al., 2016). The processes inferred from the collected data identify the riverbank as a key zone for As mobilisation.

Following the groundwater flow direction, zone B (about 200 m downstream of the riverbank in the Holocene aquifer) has As concentrations in the same range as in the riverbank pore water (120–140 μg/L), suggesting a net transport of As from zone A to B.

**Table 1**
Concentration of dissolved As and related hydrochemical parameters in groundwater measured in October 2017 at a depth of 22–25 m. This depth range was selected because the highest As concentrations were found there. The groundwater flow is from right to left. Letters A–E represent the hydro(geo)chemical zones, as indicated in Fig. 1. Background cell colours are scaled for each hydrochemical parameter to improve visual data comparability (blue for low concentration, red for high concentration, yellow for highly reducing conditions and green for mildly reducing to oxic conditions). For the river and riverbank, the average values were determined for the sample replicates collected along the Red River meander.

← **groundwater flow direction**

| | | Pleistocene aquifer (22–25 m) | | | | RTZ | | | Holocene aquifer (22-25 m) | | | Bank | River |
|---|---|---|---|---|---|---|---|---|---|---|---|---|---|
| **Geochemical zones** | | E | | | | D | | | C | B | | A | |
| **As processes** | | Pristine/Retardation | | | | Retardation | | | Mobilisation | Transport | | Mobilisation | |
| **Local well ID** | | A-24 | 2 | 4 | 36 | 32 | 31 | 11-25 | 5 | 12 | | - | - |
| **Well code used here** | | | E2 | E1 | | D2 | | D1 | C | B | | | |
| **As** | μg/L | 3.8 | 6.3 | 1.7 | 1.4 | 97 | 295 | 393 | 509 | 143 | | 123 | 2.3 |
| **Fe** | mg/L | 0.4 | 0.8 | 0.3 | 1.3 | 9.4 | 11 | 11 | 13 | 9.5 | | 6.8 | <0.05 |
| **Mn** | mg/L | 2.0 | 0.4 | 1.2 | 2.3 | 3.9 | 0.9 | 0.4 | 0.1 | 0.8 | | 7.3 | 0.0 |
| **DOC** | mgC/L | 1.4 | 2.0 | 1.7 | 1.6 | 3.4 | 3.9 | 4.0 | 9.2 | 1.5 | | 8.2 | 1.9 |
| **C-alkalinity** | mmol HCO$_3^-$/L | 2.3 | 7.0 | 8.3 | 9.5 | 10 | 10 | 9.7 | 13 | 8.5 | | 19 | 1.7 |
| **CH$_4$** | mg/L | <0.13 | <0.13 | <0.13 | 4.3 | 37 | 31 | 18 | 46 | 0.31 | | - | - |
| **NH$_4^+$** | mgN/L | 0.1 | 24 | 15 | 13 | 19 | 23 | 21 | 67 | 0.6 | | 6.2 | 0.3 |
| **PO$_4^{3-}$** | mgP/L | 0.04 | 0.10 | 0.07 | 0.03 | 0.3 | 0.4 | 0.5 | 1.6 | 0.7 | | 0.00 | 0.03 |
| **O$_2$** | mg/L | <0.05 | <0.05 | <0.05 | <0.05 | <0.05 | <0.05 | <0.05 | <0.05 | <0.05 | | - | 6.80 |
| **NO$_3^-$** | mgN/L | <0.05 | <0.05 | <0.05 | <0.05 | <0.05 | <0.05 | <0.05 | <0.05 | <0.05 | | <0.05 | 0.95 |
| **S** | mgS/L | 2.7 | <0.1 | <0.1 | <0.1 | <0.1 | <0.1 | <0.1 | 0.1 | 0.8 | | 12 | 2.5 |
| **E$_h$** | mV | 85 | 112 | 146 | 113 | 10 | 11 | 17 | 36 | 19 | | - | 408 |

This transport could be an effect of the release of As via reductive dissolution of Fe(III) (oxyhydr)oxides and the concurrent immobilisation of As by sorption and incorporation to newly formed Fe(II) sulphides and mixed valence Fe(II)/Fe(III) (oxyhydr)oxides (Smedley and Kinniburgh, 2002; Bostick and Fendorf, 2003; Sø et al., 2018a; Sø et al., 2018b). Similarly, between zones A and B, the dissolved Fe concentration shows a change from 6.8 to 9.5 mg/L. Given that groundwater is saturated with respect to siderite, this reflects a combination of continued Fe(III) reduction and a decrease in pH that affects carbonate activity. The elevated $PO_4^{3-}$ concentration (0.7 mg P/L) is consistent with the release of adsorbed P by reductive dissolution of Fe(III) minerals and its limited re-adsorption (Biswas et al., 2014; Rathi et al., 2017; Neidhardt et al., 2018a; Neidhardt et al., 2018b). Concentrations of dissolved organic carbon decrease from 8.2 mg C/L to 1.5 mg C/L, indicating that DOC released from riverbank sediments is consumed by microbial respiration. At the same time, the sulphur concentration decreases from 12 to 0.8 mg S/L, with sulphate constituting almost all the total sulphur concentration in solution (Table A1), indicating that both $SO_4^{2-}$ and Fe(III) are actively reduced between zones A and B. The products of Fe(III) and $SO_4^{2-}$ reduction include Fe and sulphide minerals, with geochemical modelling suggesting groundwater saturation with respect to these minerals. Despite $SO_4^{2-}$ reduction, the presence of excess $Fe^{2+}$ maintains dissolved S at very low concentrations in successive hydro(geo)chemical zones.

In zone C of the Holocene aquifer (about 1.6 km downstream of the riverbank), dissolved As, Fe, DOC, $NH_4^+$ and $PO_4^{3-}$ concentrations were the highest (509 μg As/L, 13 mg Fe/L, 9.2 mg C/L, 67 mg N/L and 1.6 mg P/L, respectively), and the C-alkalinity increased from 8.5 in zone B to 13 mmol $HCO_3^-$/L in zone C (DIC from 9.9 to 15.4 mmol $HCO_3^-$/L). These concurrent increases in As and other redox species suggest that they are sourced from within zone C (or its vicinity) and occur in addition to As mobilised at the riverbank and transported to zone C. High DOC, and particularly high $NH_4^+$ concentrations, indicate the presence of a second source of organic matter, and that this organic matter is mineralised. This mineralisation leads to further reduction of Fe(III) (oxyhydr)oxides, the release of associated As and $PO_4^{3-}$ and increasing $HCO_3^-$ concentrations, as well as to the onset of methanogenic conditions, with aqueous methane reaching a concentration of nearly 50 mg/L.

The presence of an additional source of organic matter has been speculated in previous studies (Berg et al., 2008; Eiche et al., 2008; van Geen et al., 2013; Eiche et al., 2017). Organic matter can be present in-aquifer as a coating on residual Fe(III) minerals and can be released in conjunction with or after their dissolution. However, aquifer sediments themselves present low concentrations of sedimentary organic matter (TOC below 0.03 wt%, Eiche et al., 2008), so a further carbon source is implicitly needed to trigger the local increase in Fe reduction. A potentially more abundant source could be discrete organic matter-rich strata of marine, freshwater or partially terrestrial origin buried in the Holocene silty aquitard with intercalated sand lenses, which was deposited on top of the aquifer (TOC variable from 0.8 wt% to 4.5 wt%, Eiche et al., 2008). The pore water in the silts was actually enriched in As (20–200 μg/L) and could also present significant amounts of DOC mobilised by organic matter degradation and Fe (oxyhydr)oxides reduction (Berg et al., 2008; Eiche et al., 2008; Kuroda et al., 2017b). The stable water isotope data presented in this study (Fig. 3) and the water ages reported in van Geen et al. (2013) are consistent with an egress of pore water from the aquitard into the aquifer in zone C, potentially supplying reactive DOC, as discussed in Section 3.1. Further assessment is required to understand (i) the extent to which As in zone C is mobilised 'in situ' from aquifer sediments, and/or is already released into the pore water of the aquitard and transported into the aquifer; and (ii) whether a direct biogeochemical link exists between methane and the Fe cycle leading to As (im)mobilisation or whether these cycles co-occur independently under highly reducing conditions.

At a 1.6 to 1.7 km distance from the riverbank (RTZ, zone D), dissolved As concentrations decrease from 393 to 97 μg/L, despite the persistence of

methane in the aquifer. Dissolved Fe and $PO_4^{3-}$ concentrations also decrease between zones C and D, from 13 to 9.4 mg Fe/L and from 1.6 to 0.3 mg P/L, respectively. Fe(II) sulphides, carbonates and Fe(II)/Fe(III) (oxyhydr)oxides can be stable under reducing conditions and might provide sufficient sorption capacity to trigger sufficient partitioning of As to affect its aqueous concentrations (Smedley and Kinniburgh, 2002; Bostick and Fendorf, 2003; Rathi et al., 2017; Neidhardt et al., 2018b; Sø et al., 2018a; Sø et al., 2018b). These minerals were previously found in the Holocene sands at the same field site, and pyrite was confirmed in the upper layers of the Pleistocene sands (Eiche et al., 2008). Similarly, the geochemical modelling of the hydrochemical data presented in this study (Section 3.2.2) points to near-saturation and saturation of groundwater with respect to Fe(II) carbonates and Fe(II)/Fe(III) (oxyhydr)oxides. Therefore, the decrease in dissolved As, Fe and $PO_4^{3-}$ concentrations in zone D might reflect a co-precipitation and sorption occurring under reducing conditions.

At 1.7 km from the riverbank, the redox potential ($E_h$) sharply increased, from +10 mV to +113 mV (between zone D and E). The RTZ is characterised by high dissolved Mn concentrations (2.3–3.9 mg Mn/L), indicating Mn(III/IV) (oxyhydr)oxides reduction. This process is likely fuelled by the advection of Fe-reducing groundwater rich in $Fe^{2+}$ and $CH_4$ and is consistent with the moderate levels of DOC, $NH_4^+$ and C-alkalinity/DIC. Dissolved $Fe^{2+}$ advected from the Fe-reducing Holocene aquifer can promote the abiotic reduction of sedimentary Mn(III/IV) with a release of $Mn^{2+}$ in solution and re-oxidation of Fe (similarly to what is reported by Gillispie et al., 2019 for Pleistocene sediments rich in Mn(III/IV) in Cambodia). This process is corroborated by the decrease in dissolved Fe and As concentrations between zones D and E. Proceeding further in the Pleistocene aquifer (zone E), the As concentrations remain below 10 μg/L and the $PO_4^{3-}$ concentrations remain below 0.15 mg/L. The groundwater hydrochemistry suggests the presence of Mn-reducing conditions that maintain relatively stable Fe(III) (oxyhydr)oxides, which have a high sorption capacity for As (Eiche et al., 2008). Nevertheless, $NH_4^+$ and DOC are still moderately abundant in zone E (0.1–24 mg N/L, 1.4–2.0 mg C/L, respectively). Dissolved organic matter has the potential to reduce Fe(III) (oxyhydr)oxides, as suggested by the maintenance of Fe concentrations in solution between 0.4 and 1.3 mg/L.

### 3.3. Temporal evolution of arsenic contamination

#### 3.3.1. Temporal changes of groundwater sources

The ternary diagrams for cations and anions (Fig. 5) provide insights into the hydrochemistry between 2010 and 2017. We focused on wells located in the hydro(geo)chemical zones described above (including data from Neidhardt et al., 2018a), with a screen of 22–25 m depth, for which temporal data are available.

The groundwater along the studied transect is of $Ca^{2+}/Mg^{2+}$-$HCO_3^-$ type, confirming the overall presence of freshwater and the dissolution of $Ca^{2+}$ and $Mg^{2+}$ carbonates that buffer the acidity related to the oxidation of organic carbon, as described in Section 3.2.1. In agreement with the previous results discussed in Section 3.2.3, we found that the aquifer zone B is mainly replenished by riverbank water, with a varying relative contribution of dissolved $SO_4^{2-}$ (Fig. 5b). This likely reflects a temporal variability of the spatial extent of sulphate reduction between zone A and zone B.

The enrichment in the relative abundance of Na + K for wells in zone C, D and E indicates a further source of water in addition to riverbank water. Both Holocene and Pleistocene aquifer sands contain feldspar and mica (Eiche et al., 2008), which could contribute to an increase in the relative abundance of Na + K after weathering. Further Na and K sources could include evaporative water, which could be richer in K originating from fertilisers (Fig. 5a). We strove to disentangle these sources by separating the relative contribution of Na and K by comparing the molar ratios K/Ca and Na/Ca (Fig. 5c). The well in zone C, Holocene aquifer, lies on the mixing line of the riverbank and pond water, which is
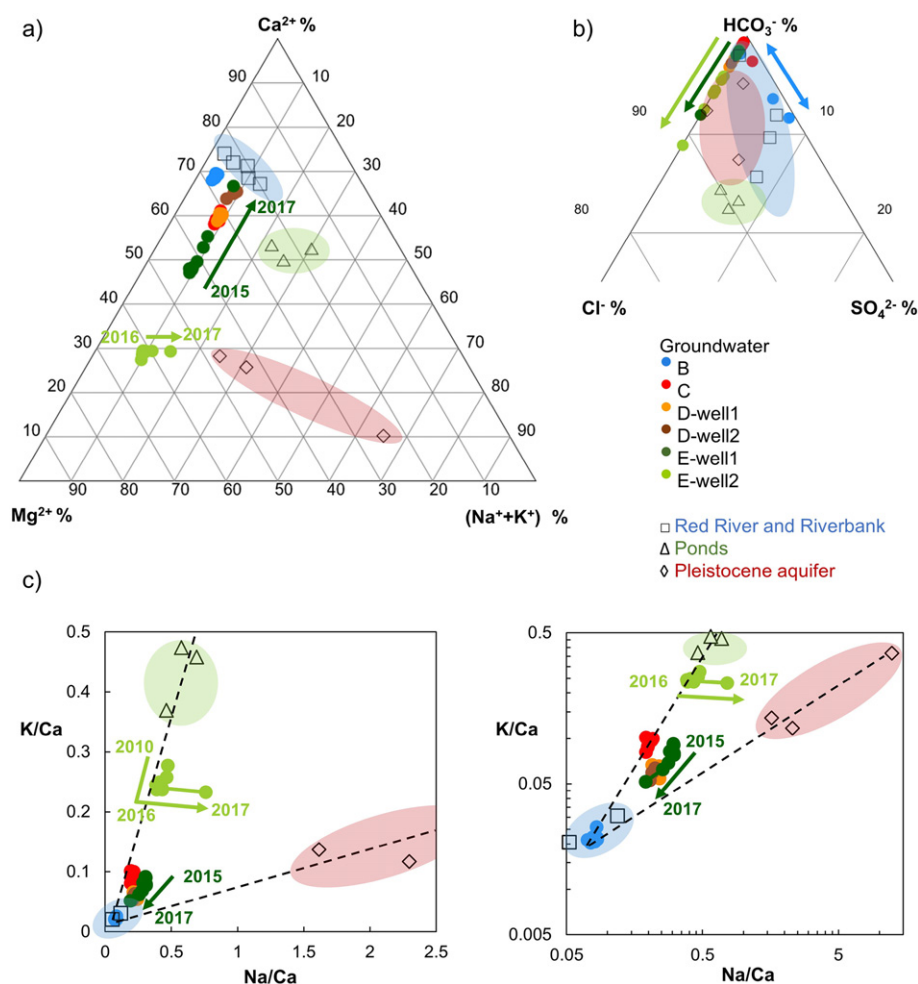
**Fig. 5.** a) Cation and b) anion ternary diagrams of monitoring data from 2010 to 2017, c) bivariate cation ratios (log scale on the lower right panel) showing the major ion composition of groundwater in the different zones (dots, from B to E). Arrows indicate changes over the period 2010–2017. The end members of water sources are indicated by colour: river and riverbank samples (empty squares, blue area), surface ponds (empty triangles, green area), and background Pleistocene wells (empty diamonds, red area). The wells tapping the Pleistocene aquifer at a 2 km distance from the riverbank were taken as the best available reference of Pleistocene hydro(geo)chemistry (nested well on the left in Figs. 3 and 4; A-24, A-38 and A-54 in Table A1). The ternary diagrams were generated using the PAST software for multivariate statistics.

further indicative of evaporative water infiltration through the aquitard in zone C. The groundwater composition of zone D plots between the two mixing lines of the riverbank-pond and riverbank-Pleistocene, suggesting a fraction of Pleistocene water in the RTZ. Interestingly, well D-1 shows the same type of water as is found in the well in zone C Holocene aquifer (Fig. 5a, orange and red dots overlap for time series). Well D-2, located only about 25 m downstream of D-1, has a water composition that is intermediate between zones C-D1 and riverbank water. This indicates the possibility of a preferential or transverse flow of groundwater from different sources that creates heterogeneity in groundwater composition in zone D and that likely bypasses the wells in zones C and D-1.

The largest hydro(geo)chemical temporal variability was observed for the wells in zone E. This is expected, given the increased contribution of local recharge within this area; however, the temporal changes suggest that this heterogeneity may be transient. Well E-1 has been receiving more groundwater from zone D and the riverbank since 2015, confirming the connection with zone D and pointing further to the possibility of a flow of water from the riverbank around zone C, progressively merging in zone D, (well D-2) and zone E (well E-1). Well E-2 has recently progressed from a mixed riverbank and evaporative composition towards more Pleistocene-like conditions (Fig. 5a), indicating a local alteration in the groundwater flow direction that is potentially caused by the steadily increasing pumping activities in Van Phuc village.

The absence of a comparable temporal hydro(geo)chemical change indicates more constant conditions in zones C and D and a more uniform mix of water sources. An additional feature of zones C and D is the presence of methane concentrations from 18 to 50 mg $CH_4/L$ (Section 3.2.3). Methane could form gas pockets, thereby reducing the groundwater flow and making an additional contribution to the temporal stability of zones C and D. As a very first approach to test this hypothesis, the fugacity (the gas equivalent of the SI) values for methane were calculated using PHREEQC. The chosen values were of 25–26 °C for the measured groundwater temperature (Table A1) and 2.5 atm for the pressure (atmospheric pressure plus an average of 15 m water column, as the difference between the groundwater table at 8 m depth and the well screen at 23–24 m depth). The results indicate a fugacity for methane of −0.14 to 0.27 at near-saturation conditions. Therefore, methane could form interstitial gas pockets and cause local disruptions in the groundwater flow.

### 3.3.2. Temporal variability of As concentrations and stable water isotopes

Arsenic showed little intra-annual variation for most wells in our time series from 2010 to 2017 (Fig. 6). In fact, water flows through the confined aquifer at an average speed of 40 m/year, according to van Geen et al. (2013), and a certain degree of mixing and smoothing of seasonal variations can be expected. Indeed, no increase has been observed in dissolved As at the RTZ (zone D) and no breakthrough of As exceeding
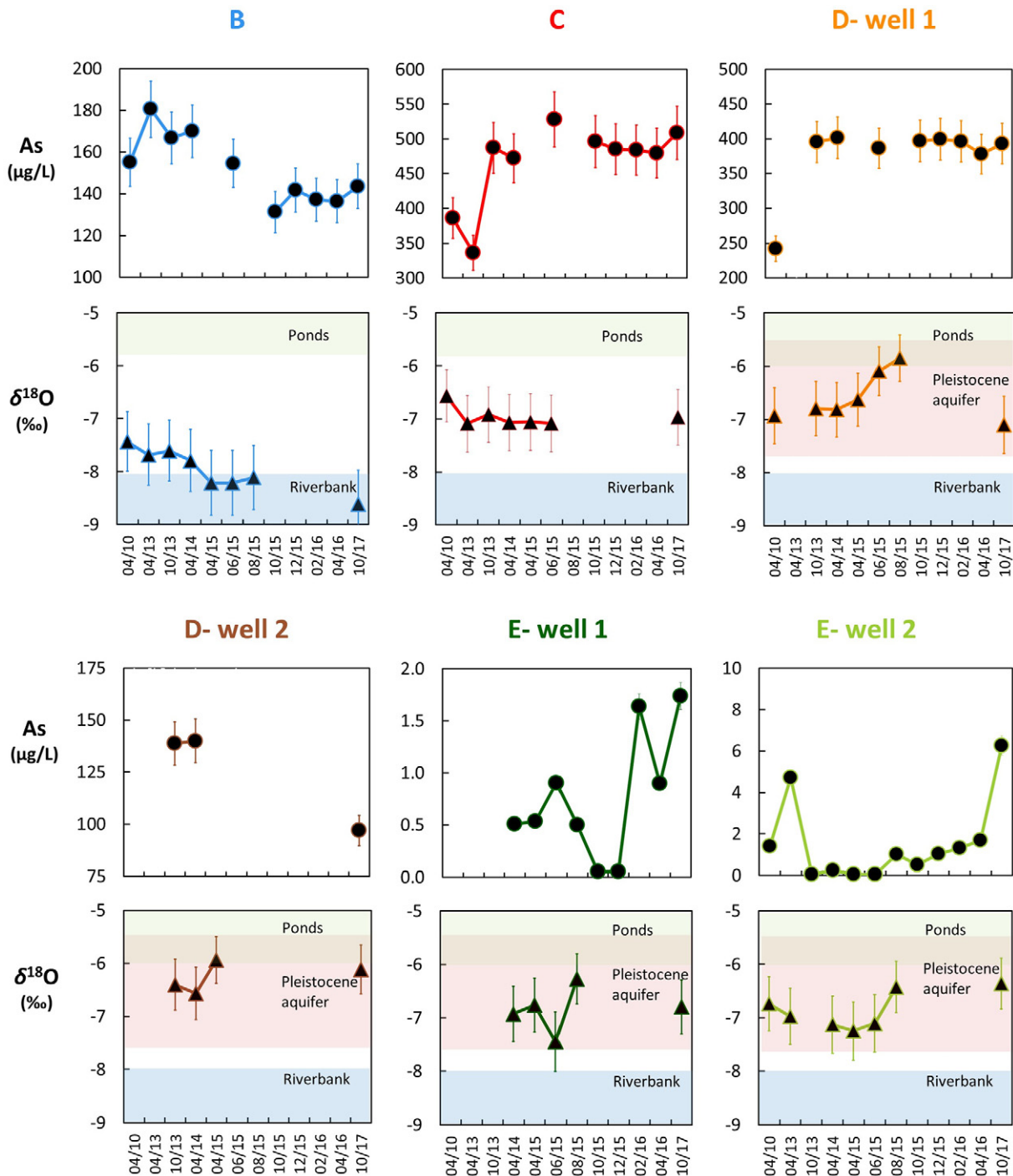
**Fig. 6.** Time series of dissolved As and $\delta^{18}O$ values of the hydro(geo)chemical zones. The $\delta^{18}O$ panels show the isotopic range of the different water sources defined in Section 3.3.1, based on the available data as reported in Table A1 and Fig. 2. Note that the range of As concentrations on the y-axes varies in each plot to facilitate comparison of the data. Factors such as differences in sampling conditions, sample preservation strategy and changes in operators are potentially affecting the comparability of results for different sampling campaigns. Therefore, we mostly refer to overall trends and associate a conservative 15% variability to the data points.

10 μg/L has been noted in the downgradient Pleistocene wells (zone E) at 22–25 m depths during the last 8 years. This indicates that As sorption in the RTZ is preventing/retarding the intrusion of As into the Pleistocene aquifer. A closer look at the temporal data in Fig. 6 helps to quantify the responsiveness of the Holocene and Pleistocene aquifers with respect to As advection.

In zone B, at the well closest to the river, the dissolved As concentration was 30–40 μg/L higher in 2010–2013 than in 2016–2017. As discussed in Section 3.3.1, the aquifer at zone B is mainly fed by water from the riverbank. At the same time, the $\delta^{18}O$ values decreased from

−7.6‰ to −8.6‰, coinciding with larger volumes of river water infiltration caused by the steady increase in groundwater abstractions in Hanoi (Giao et al., 2018). The larger amount of river infiltrate leads to somewhat lower As concentrations by the flushing of As present in the riverbank pore water (zone A), but it preserves the relative abundance of cations in zone B (Figs. 5 and 6).

Further downstream, in the Holocene aquifer (zone C), the As level increased from 380 μg/L to 450–500 μg/L in the period 2010–2013. Here, the $\delta^{18}O$ values have remained constant at −7‰, consistent with a groundwater derived from riverine and evaporative recharge,

which has sustained iron reduction and As release even in the Holocene aquifer.

The $\delta^{18}O$ signatures of groundwater at the RTZ D are indicative of a mixture of evaporative water infiltration and water of the Pleistocene aquifer, in addition to the water advected from zone C of the Holocene aquifer, as discussed in the Section 3.3.1. Dissolved As concentrations in well D-1 have been constant since 2013 at around 400 μg/L, confirming that this well is mostly impacted by advective transport from zone C. However, in well D-2 of the RTZ, the As level dropped from 140 μg/L in 2013 to 97 μg/L in 2017. This decrease of dissolved As could reflect the oxidation of dissolved $Fe^{2+}$ coupled with the reduction of Mn(III/IV) (oxyhydr)oxides in the Pleistocene sediments (as discussed in Section 3.2.3). This process results in the enrichment of Fe(III) precipitates at the RTZ, thereby enhancing the As sorption capacity and attenuation (Stollenwerk et al., 2007; Vencelides et al., 2007).

The influence of several local water sources in zone E hampers the interpretation of $\delta^{18}O$ values. Although the dissolved As level was always below 10 μg/L in the observed period from 2010 to 2017, it increased towards 2017 in both wells (E-1 and E-2). In addition, ongoing hydrochemical changes and the presence of DOC and $NH_4^+$ in zone E (Sections 3.2.3 and 3.3.1) indicate the occurrence of active redox cycling, which has the potential to trigger Fe-reducing conditions. This situation emphasises the need for close monitoring of As concentrations in the Pleistocene aquifer.

## 4. Implications

Based on the studied transect, five hydro(geo)chemical zones of As mobilisation and retardation were identified (Fig. 7).

Some hydrochemical parameters provided important information for the interpretation of the spatial and temporal patterns of dissolved As in groundwater. First, stable water isotopes and alkali cations, as well as their evolution over time, were essential for identification of the spatial patterns of water sources infiltrating into the aquifer. Second, a considerable part of the variability in dissolved As concentration could be approximated by the combination of the redox potential $E_h$ and $PO_4^{3-}$ concentration. However, the validity of this empirical relationship would need to be tested in other regions. If it held true, it could provide a low-budget and simple proxy for possible As contamination using field sensors ($E_h$) and photometry ($PO_4^{3-}$) in areas where equipment for As analysis is not in place. Third, dissolved Mn is abundant where dissolved $Fe^{2+}$ advected from the Fe-reducing Holocene aquifer causes an abiotic reduction of the sedimentary Mn(III/IV) oxides in Pleistocene sediments. We suggest that dissolved Mn is indicative of environments actively undergoing reduction and provides an indication of the current position of the RTZs boundary and early warning for the potential future spread of dissolved As.

The hydro(geo)chemical zones describing As mobilisation and retardation indicate an interplay of processes responsible for the local-scale variability ($10^1$ to $10^2$ m) of groundwater As concentrations (Table 2), involving several redox couples and element cycles (Fe, S, Mn and organic C). The studied aquifer/aquitard architecture is characterised by features typical of other regions in South and East Asia affected by high As levels in groundwater, with overlying Holocene and Pleistocene aquifers and RTZs between high- and low-As groundwater. Therefore, the proposed scheme of hydro(geo)chemical zones (all or in part) is a useful conceptual guideline for the investigation of As propagation in reducing aquifer environments.

## 5. Outlook

Our study confirms significant As mobilisation from riverbank sediments and indicates further As release associated with methanogenic conditions. Stable water isotopes revealed the percolation of evaporative water through the organic matter-rich aquitard into the Holocene aquifer. As a consequence, additional dissolved organic matter is advected to the aquifer, triggering methanogenic conditions and net As mobilisation. Similarly, the egression of organic matter-rich water can occur in regions where Holocene and Pleistocene sediments are stacked vertically, especially under pumping-induced advected flow conditions, enhancing highly reducing conditions and the risk of As mobilisation in dissolved As-free pristine aquifers.

The saturation of methane in groundwater can lead to the formation of gas phase in the aquifer, hampering the groundwater flow, or even cause locally stagnant conditions. Such situations should be considered in the assessment of As in many other regions because this may lead to unpredictable changes in the groundwater flow. Similarly, the presence of gravel layers and their hydrological connection with sandy aquifers must be assessed in As contaminated regions, since gravel can constitute a further 'highway' for the transport of dissolved As.

The RTZ was stable over the study period 2010–2017, buffering As intrusion in the Pleistocene aquifer. However, the Pleistocene aquifer has undergone changes in groundwater hydrochemical composition in recent years. This is critical and calls for concerted biogeochemical research on the quantitative impact of Fe, Mn, methane and organic matter on the long-term As retardation capacity of the RTZ under different groundwater resource management scenarios.

Taking these points into consideration, a multidisciplinary project is currently carried out at this field site (project AdvectAs: Retardation and mobilisation of As at redox fronts under advective flow conditions – A
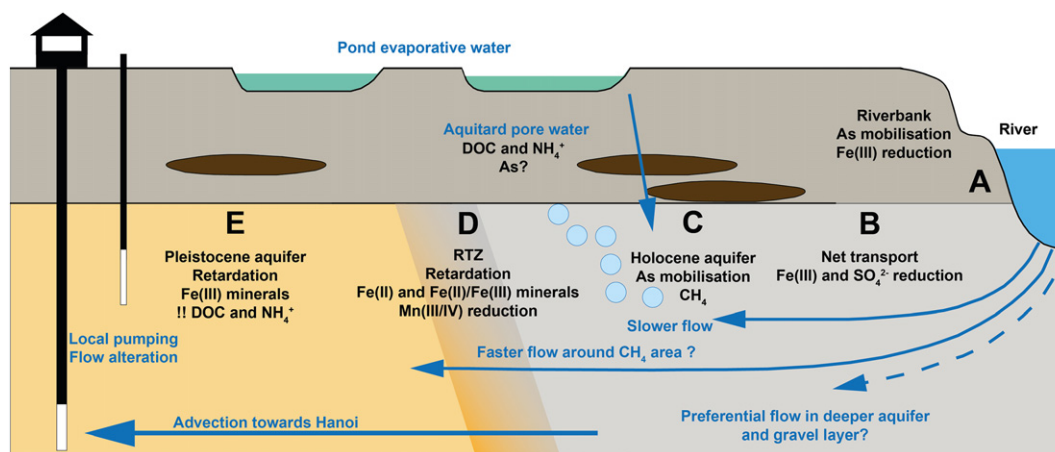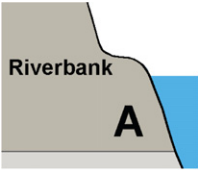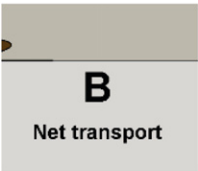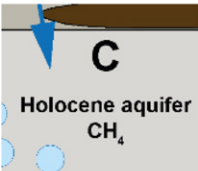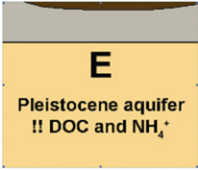


**Fig. 7.** Conceptual scheme of hydro(geo)chemical zones (A to E) involved in As mobilisation and transport through a Holocene aquifer, followed by a redox transition zone RTZ and groundwater advection into a Pleistocene aquifer. The blue arrows indicate simplified directions of the groundwater flow.

**Table 2**

Hydro(geo)chemical zones involved in groundwater As mobilisation, transport and retardation under advective conditions.

| Hydro(geo)chemical zone | As processes | Characteristics |
|---|---|---|
|  Riverbank **A** | Mobilisation | Dominant in depositional meanders; <br><br> Infiltration of river water into the aquifer is the main source of groundwater recharge; <br><br> Organic matter is abundant in young sedimentary depositions of the riverbank where As is easily mobilised; <br><br> Fe(III) reducing conditions often prevail in the sediments at depths of just a few centimetres to metres. |
|  **B** Net transport | Net transport | Holocene aquifer, low in dissolved and sedimentary organic carbon; <br><br> Fe(III) and $SO_4^{2-}$ reducing conditions; <br><br> Counteracting processes of reductive As dissolution and sorption/incorporation of As to newly formed iron- and sulphur phases occur simultaneously and are more or less balanced. |
|  **C** Holocene aquifer $CH_4$ | Mobilisation | (Re)fuelling of organic matter from vertical infiltration (percolation) of water from the aquitard and/or organic matter inclusions in Fe-oxidising sediments that breakup during Fe reduction; <br><br> If enough organic matter is present, this triggers the onset of methanogenic conditions with net As mobilisation; <br><br> Methane production can lead to oversaturation and two phase presence, with interstitial gas that might disrupt groundwater flow. |
|  **D** Transition zone | Retardation | Redox transition zone with change from Fe-/sulphate-reducing and methanogenic to Mn-reducing conditions; <br><br> Advection/intrusion of reduced groundwater from the Holocene aquifer to the Pleistocene aquifer; <br><br> Progressive sorption/incorporation of As: <br> first under highly reducing conditions to Fe(II) and Fe(II)/Fe(III) minerals; <br> then by the oxidation of dissolved Fe(II) and precipitation of Fe(III) minerals coupled with Mn(III/IV) reduction. |
|  **E** Pleistocene aquifer !! DOC and $NH_4^+$ | Retardation | Pleistocene aquifers, widely tapped for the extraction of low-As groundwater and/or irrigation; <br><br> Moderate Mn-reducing conditions and sorption of As to Fe(III) (oxyhydr)oxides; <br><br> Presence of DOC and $NH_4^+$ accompanied by observed temporal hydrochemical changes, implicate vulnerability of these aquifers to long-term As contamination. |

concerted multidisciplinary approach). The study combines geochemical, microbial, mineralogical and hydrological tools, as well as their integration in reactive transport modelling.

**Declaration of competing interest**

**Appendix A. Supplementary data**

Supplementary data to this article can be found online at https://doi.org/10.1016/j.scitotenv.2020.137143.

**References**

Appelo, C.A.J., Postma, D., 2005. Geochemistry, Groundwater and Pollution. 2nd edition. CRC Press, Boca Raton.

Berg, M., Tran, H.C., Nguyen, T.C., Viet, P.H., Schertenleib, R., Giger, W., 2001. Arsenic contamination of groundwater and drinking water in Vietnam: a human health threat. Environ. Sci. Technol. 35, 2621–2626. https://doi.org/10.1021/es010027y.

Berg, M., Stengel, C., Trang, P.T.K., Viet, P.H., Sampson, M.L., Leng, M., Samreth, S., Fredericks, D., 2007. Magnitude of arsenic pollution in the Mekong and Red River Deltas — Cambodia and Vietnam. Sci. Total Environ. 372, 413–425. https://doi.org/10.1016/j.scitotenv.2006.09.010.

Berg, M., Trang, P.K.T., Stengel, C., Buschmann, J., Viet, P.H., Dan, N.V., Giger, W., Stüben, D., 2008. Hydrological and sedimentary controls leading to arsenic contamination of groundwater in the Hanoi area, Vietnam: the impact of iron-arsenic ratios, peat,

river bank deposits, and excessive groundwater abstraction. Chem. Geol. 249, 91–112. https://doi.org/10.1016/j.chemgeo.2007.12.007.

Biswas, A., Gustafsson, J.P., Neidhardt, H., Halder, D., Kundu, A.K., Chatterjee, D., Berner, Z., Bhattacharya, P., 2014. Role of competing ions in the mobilization of arsenic in groundwater of Bengal Basin: insight from surface complexation modelling. Water Res. 55, 30–39. https://doi.org/10.1016/j.watres.2014.02.002.

Bostick, B.C., Fendorf, S., 2003. Arsenite sorption on troilite (FeS) and pyrite (FeS$_2$). Geoch. Cosmoch. Acta 67, 909–921. https://doi.org/10.1016/S0016-7037(02)01170-5.

Buschmann, J., Berg, M., Stengel, C., Winkel, L., Sampson, M.L., Trang, P.T.K., Viet, P.H., 2008. Contamination of drinking water resources in the Mekong delta floodplains: arsenic and other trace metals pose serious health risks to population. Environ. Int. 34, 756–764. https://doi.org/10.1016/j.envint.2007.12.025.

Eiche, E., Neumann, T., Berg, M., Weinmann, B., van Geen, A., Norra, S., Berner, Z., Trang, P.K.T., Viet, P.H., Stüben, D., 2008. Geochemical processes underlying a sharp contrast in groundwater arsenic concentrations in a village on the Red River delta, Vietnam. Appl. Geochem. 23, 3143–3154. https://doi.org/10.1016/j.apgeochem.2008.06.023.

Eiche, E., Berg, M., Hönig, S.-M., Neumann, T., Lan, V.M., Trang, P.K.T., Viet, P.H., 2017. Origin and availability of organic matter leading to arsenic mobilisation in aquifers of the Red River Delta, Vietnam. Appl. Geochem. 77, 184–193. https://doi.org/10.1016/j.apgeochem.2016.01.006.

Fendorf, S., Michael, H.A., van Geen, A., 2010. Spatial and temporal variations of groundwater arsenic in South and Southeast Asia. Science Review 328, 1123–1127. https://doi.org/10.1126/science.1172974.

Giao, P.H., Hue, V.T., Han, N.D., Anh, N.T.H., Minh, N.N., 2018. Land subsidence prediction for a new urban mass rapid transit line in Hanoi. Underground Space https://doi.org/10.1016/j.undsp.2018.11.002.

Gillispie, E.C., Matteson, A.R., Duckworth, O.W., Neumann, R.B., Phen, N., Polizzotto, M.L., 2019. Chemical variability of sediment and groundwater in a Pleistocene aquifer of Cambodia: implications for arsenic pollution potential. Geoch. Cosmoch. Acta 245, 441–458. https://doi.org/10.1016/j.gca.2018.11.008.

Hammer, Ø., Harper, D.A.T., Ryan, P.D., 2001. PAST: paleontological statistics software package for education and data analysis. Palaeontol. Electron., 4 Available at. https://folk.uio.no/ohammer/past/.

Harvey, C.F., Swartz, C.H., Badruzzaman, A.B.M., Blute, N.K., Yu, W., Ali, M.A., Jay, J., Beckie, R., Niedan, V., Brabander, D., Oates, P.M., Ashfaque, K.N., Islam, S., Hemond, H.F., Ahmed, M.F., 2002. Arsenic mobility and groundwater extraction in Bangladesh. Science 298, 1602–1606. https://doi.org/10.1126/science.1076978.

Hug, S.J., Gaertner, D., Roberts, L.C., Schirmer, M., Ruettimann, T., Rosenberg, T.M., Badruzzaman, A.B.M., Ali, M.A., 2011. Avoiding high concentrations of arsenic, manganese and salinity in deep tubewells in Munshiganj District, Bangladesh. Appl. Geochem. 26, 1077–1085. https://doi.org/10.1016/j.apgeochem.2011.03.012.

Kapaj, S., Peterson, H., Liber, K., Bhattacharya, P., 2006. Human health effects from chronic arsenic poisoning– a review. J. Environ. Sci. Heal. A 41, 2399–2428. https://doi.org/10.1080/10934520600873571.

Kuroda, K., Hayashi, T., Do, A.T., Canh, V.D., Nga, T.T.V., Funabiki, A., Takizawa, S., 2017a. Groundwater recharge in suburban areas of Hanoi, Vietnam: effect of decreasing surface-water bodies and land-use change. Hydrogeol. J. 25, 727–742. https://doi.org/10.1007/s10040-016-1528-2.

Kuroda, K., Hayashi, T., Funabiki, A., Do, A.T., Canh, V.D., Nga, T.T.V., Takizawa, S., 2017b. Holocene estuarine sediments as a source of arsenic in Pleistocene groundwater in suburbs of Hanoi, Vietnam. Hydrogeol. J. 25, 1137–1152. https://doi.org/10.1007/s10040-016-1527-3.

Lawson, M., Polya, D.A., Boyce, A.J., Bryant, C., Mondal, D., Shantz, A., Ballentine, C., 2013. Pond-derived organic carbon driving changes in arsenic hazard found in Asian groundwaters. Env. Sci. Technol. 47, 7085–7094. https://doi.org/10.1021/es400114q.

McArthur, J.M., Banerjee, D.M., Sengupta, S., Ravenscroft, P., Klump, S., Sarkar, A., Disch, B., Kipfer, R., 2010. Migration of As, and $^3$H/$^3$He ages, in groundwater from West Bengal: implications for monitoring. Water Res. 44, 4171–4185. https://doi.org/10.1016/j.watres.2010.05.010.

Meng, X., Wang, W., 1998. Speciation of arsenic by disposable cartridges. Conference Contribution to the Third International Conference on Arsenic Exposure and Health Effects, San Diego, CA, July 12–15.

Neidhardt, H., Schoeckle, D., Schleinitz, A., Eiche, E., Berner, Z., Trang, P.K.T., Lan, V.M., Viet, P.H., Biswas, A., Majumder, S., Chatterjee, D., Oelmann, Y., Berg, M., 2018a. Biogeochemical phosphorus cycling in groundwater ecosystems – insights from South and Southeast Asian floodplain and delta aquifers. Sci. Total Environ. 644, 1357–1370. https://doi.org/10.1016/j.scitotenv.2018.07.056.

Neidhardt, H., Winkel, L.H.E., Kaegi, R., Stengel, C., Trang, P.T.K., Lan, V.M., Viet, P.H., Berg, M., 2018b. Insights into arsenic retention dynamics of Pleistocene aquifer sediments by in situ sorption experiments. Water Res. 129, 123–132. https://doi.org/10.1016/j.watres.2017.11.018.

Nghiem, A.A., Stahl, M.O., Mailloux, B.J., Mai, T.T., Trang, P.T., Viet, P.H., Harvey, C.F., van Geen, A., Bostick, B.C., 2019. Quantifying riverine recharge impacts on redox conditions and arsenic release in groundwater aquifers along the Red River, Vietnam. Water Resour. Res. 55, 6712–6728. https://doi.org/10.1029/2019WR024816.

Parkhurst, D.L., Appelo, C.A.J., 2013. Description of input and examples for PHREEQC version 3—a computer program for speciation, batch-reaction, one-dimensional

transport, and inverse geochemical calculations. U.S. Geological Survey Techniques and Methods book 6, chap. A43, 497 p. Available at. https://pubs.usgs.gov/tm/06/a43/.

Podgorski, J.E., Eqani, S.A.M.A.S., Khanam, T., Ullah, R., Shen, H., Berg, M., 2017. Extensive arsenic contamination in high-pH unconfined aquifers in the Indus Valley. Sci. Adv. 3, e1700935. https://doi.org/10.1126/sciadv.1700935.

Polya, D., Charlet, L., 2009. Rising arsenic risk? Nat. Geosci. 2, 383–384. https://doi.org/10.1038/ngeo537.

Polya, D., Sparrenbom, C., Datta, S., Guo, H., 2019. Groundwater arsenic biogeochemistry – key questions and use of tracers to understand arsenic-prone groundwater systems. Geosci. Front. 10, 1635–1641. https://doi.org/10.1016/j.gsf.2019.05.004.

Postma, D., Larsen, F., Thai, N.T., Trang, P.T.K., Jakobsen, R., Nhan, P.Q., Long, T.V., Viet, P.H., Murray, A.S., 2012. Groundwater arsenic concentrations in Vietnam controlled by sediment age. Nat. Geosci. 5, 656–661. https://doi.org/10.1038/NGEO1540.

Rathi, B., Neidhardt, H., Berg, M., Siade, A., Prommer, H., 2017. Processes governing arsenic retardation on Pleistocene sediments: adsorption experiments and model-based analysis. Water Resour. Res. 53, 4344–4360. https://doi.org/10.1002/2017WR020551.

Rawson, J., Prommer, H., Siade, H., Carr, J., Berg, M., Davis, J.A., Fendorf, S., 2016. Numerical modeling of arsenic mobility during reductive iron-mineral transformations. Env. Sci. Technol. 50, 2459–2467. https://doi.org/10.1021/acs.est.5b05956.

Rawson, J., Siade, A., Sung, J., Neidhardt, H., Berg, M., Prommer, H., 2017. Quantifying reactive transport processes governing arsenic mobility after injection of reactive organic carbon into a Bengal Delta aquifer. Env. Sci. Technol. 51, 8471–8480. https://doi.org/10.1021/acs.est.7b02097.

Richards, L.A., Mangone, D., Sovann, C., Kong, C., Uhlemann, S., Kuras, O., van Dongen, B.E., Ballentine, C.J., Polya, D.A., 2017. High resolution profile of inorganic aqueous geochemistry and key redox zones in an arsenic bearing aquifer in Cambodia. Sci. Total Environ. 590–591, 540–553. https://doi.org/10.1016/j.scitotenv.2017.02.217.

Rodriguez-Lado, L., Sun, G., Berg, M., Zhang, Q., Xue, H., Zheng, Q., Johnson, C.A., 2013. Groundwater arsenic contamination throughout China. Science 341, 866–868. https://doi.org/10.1126/science.1237484.

Smedley, P.L., Kinniburgh, D.G., 2002. A review of the source, behaviour and distribution of arsenic in natural waters. Appl. Geochem. 17, 517–568. https://doi.org/10.1016/S0883-2927(02)00018-5.

Sø, H.U., Postma, D., Hoang, V.H., Lan, V.M., Trang, P.T.K., Viet, P.H., Jakobsen, R., 2018a. Arsenite adsorption controlled by the iron oxide content of Holocene Red River aquifer sediment. Geoch. Cosmoch. Acta 239, 61–73. https://doi.org/10.1016/j.gca.2018.07.026.

Sø, H.U., Postma, D., Lan, V.M., Trang, P.T.K., Kazmierczak, J., Nga, D.V., Pi, K., Koch, C.B., Viet, P.H., Jakobsen, R., 2018b. Arsenic in Holocene aquifers of the Red River floodplain, Vietnam: effects of sediment-water interactions, sediment burial age and groundwater residence time. Geoch. Cosmoch. Acta 225, 192–209. https://doi.org/10.1016/j.gca.2018.01.010.

Sracek, O., Berg, M., Müller, B., 2018. Redox buffering and de-coupling of arsenic and iron in reducing aquifers across the Red River Delta, Vietnam, and conceptual model of de-coupling processes. Environ. Sci. Pollut. Res. 25, 15954–15961. https://doi.org/10.1007/s11356-018-1801-0.

Stahl, M.O., Harvey, C.F., van Geen, A., Sun, J., Trang, P.K.T., Lan, V.M., Phuong, T.M., Viet, P.H., Bostick, B.C., 2016. River bank geomorphology controls groundwater arsenic concentrations in aquifers adjacent to the Red River, Hanoi Vietnam. Water Resour. Res. 52 (8), 6321–6334. https://doi.org/10.1002/2016WR018891.

Stollenwerk, K.G., Breit, G.N., Welch, A.H., Yount, J.C., Whitney, J.W., Foster, A.L., Uddin, M.N., Majumder, R.K., Ahmed, N., 2007. Arsenic attenuation by oxidized aquifer sediments in Bangladesh. Sci. Total Environ. 379, 133–150. https://doi.org/10.1016/j.scitotenv.2006.11.029.

Tanabe, S., Horib, K., Saitoc, Y., Haruyamad, S., Vue, V.P., Kitamura, A., 2003. Song Hong (Red River) delta evolution related to millennium-scale Holocene sea-level changes. Quaternary Sci. Rev. 22, 2345–2361. https://doi.org/10.1016/S0277-3791(03)00138-0.

van Geen, A., 2011. International drilling to recover aquifer sands (IDRAs) and arsenic contaminated groundwater in Asia. Sci. Drill. 12, 49–52. https://doi.org/10.2204/iodp.sd.12.06.2011.

van Geen, A., Bostick, B.C., Trang, P.K.T., Lan, V.M., Mai, N.-N., Manh, P.D., Viet, P.H., Radloff, K., Aziz, Z., Mey, J.L., Stahl, M.O., Harvey, C.F., Oates, P., Weinmann, B., Stengel, C., Frei, F., Kipfer, R., Berg, M., 2013. Retardation of arsenic transport through a Pleistocene aquifer. Nature 501, 204–207. https://doi.org/10.1038/nature12444.

Vencelides, Z., Sracek, O., Prommer, H., 2007. Modelling of iron cycling and its impact on the electron balance at a petroleum hydrocarbon contaminated site in Hnevice, Czech Republic. J. Contamin. Hydrol. 89, 270–294. https://doi.org/10.1016/j.jconhyd.2006.09.003.

WHO, 2011. Guidelines for Drinking-water Quality. 4th edition. (Geneva).

Winkel, L., Berg, M., Amini, M., Hug, S.J., Johnson, A., 2008. Predicting groundwater arsenic contamination in Southeast Asia from surface parameters. Nat. Geosci. 11, 536–542. https://doi.org/10.1038/ngeo254.

Winkel, L.H.E., Pham, T.K.T., Lan, V.M., Stengel, C., Aminia, M., Hac, N.T., Viet, P.H., Berg, M., 2011. Arsenic pollution of groundwater in Vietnam exacerbated by deep aquifer exploitation for more than a century. PNAS 108 (4), 1246–1251. https://doi.org/10.1073/pnas.1011915108.